

Georges R. Younes, A. Jeffrey Giacomin* and Peter H. Gilbert

Temperature rise in a verging annular die

DOI 10.1515/polyeng-2015-0382

Received September 8, 2015; accepted September 28, 2015; previously published online December 19, 2015

Abstract: Plastic pipes, tubes or catheters are extruded by pressure-driven flows through annular dies. Whereas die lands are straight, the section connecting the die land to the extruder either converges or diverges, converging when the product is smaller than the extruder barrel, and diverging when larger. In this paper, we carefully consider the converging or diverging connecting flows, in spherical coordinates, for the most common configuration: the Newtonian pressure-driven flow through the annulus between two coapical coaxial cones. We derive the *exact* analytical solution for the velocity profile, and then use this to arrive at the *exact* analytical solution for the temperature rise caused by viscous heating. We care about this rise because it often governs maximum throughput, since pipe makers must protect the melt from thermal degradation. We find that both the velocity profile, and the temperature profile, peak over the same conical surface and this surface is nearer the inner die wall. We also provide analytical expressions for the non-linear pressure profile and the die cooling requirement. We find that this cooling requirement is always higher on the inner cone.

Keywords: coaxial coapical conical dies; diverging annular die; extrudate temperature rise; plastic pipe extrusion; viscous dissipation.

*Corresponding author: A. Jeffrey Giacomin, Chemical Engineering Department, Queen's University, Kingston, ON K7L 3N6, Canada; Polymers Research Group, Queen's University, Kingston, ON K7L 3N6, Canada; and Mechanical and Materials Engineering Department, Queen's University, Kingston, ON K7L 3N6, Canada, e-mail: giacomini@queensu.ca. <http://orcid.org/0000-0002-3561-0349>

Georges R. Younes: Chemical and Petroleum Engineering Department, American University of Beirut, Riad El Solh, Beirut, 1107 2020, Lebanon; and Polymers Research Group, Queen's University, Kingston, ON K7L 3N6, Canada. <http://orcid.org/0000-0001-9425-8886>

Peter H. Gilbert: Chemical Engineering Department, Queen's University, Kingston, ON K7L 3N6, Canada; and Polymers Research Group, Queen's University, Kingston, ON K7L 3N6, Canada. <http://orcid.org/0000-0003-1707-7517>

1 Introduction

Plastic pipes, tubes, catheters or hollow fibers are extruded by pressure-driven flows through annular dies. Whereas die lands are straight, the section connecting the die land to the extruder either converges or diverges, converging when the product is smaller than the extruder barrel, and diverging when larger. We call flows that converge or diverge, *verging flows*. In this paper, we carefully consider the verging connecting flow, in spherical coordinates, for the most common configuration: the pressure-driven flow through the annulus between two coapical coaxial cones. We explore the analytical solution for the velocity profile, and then use this to calculate the temperature rise caused by viscous dissipation. We care about this rise because it often governs maximum throughput, since pipe makers must keep the melt from degrading. In this paper, we focus specifically on highly viscous nearly Newtonian polymer melts such as extrusion grades of condensation polymers. These would include nylon, polycarbonate or polyester.

Table 1 classifies the literature on pressure-driven converging or diverging annular flow. Whereas the straight annular pipe die lands are rarely concentric (a sag compensating measure [8–19]), connecting verging flow geometries are normally coapical and coaxial. Table 2 lists our dimensional variables, and Table 3, the dimensionless ones.

Parnaby and Worth [3] (see also Problems 5–37 and 5–38 of [20]) used cylindrical coordinates to arrive at the approximate analytical solution for coapical and coaxial converging annular flow of Newtonian fluids, rewritten in spherical coordinates defined in Figure 1 and Table 2 and mindful of our erratum in [3]:

$$\frac{2\mu Q(1-\kappa^3)}{3\pi\Omega r_i^3 \cos^3\theta_o \tan^4\theta_o} < \Delta p < \frac{2\mu Q(1-\kappa^3)}{3\pi\Omega r_i^3 \cos^3\theta_i \tan^4\theta_o} \quad (1)$$

where:

$$\kappa \equiv \frac{r_i}{r_o} \quad (2)$$

and for $(\tan\theta_i/\tan\theta_o) > 0.6$:

$$\Omega \equiv \frac{1}{6} \left(1 + \frac{\tan\theta_i}{\tan\theta_o} \right) \left(1 - \frac{\tan\theta_i}{\tan\theta_o} \right)^3 \quad (3)$$

Table 1: Literature on pressure-driven converging or diverging annular flow.

Papers	Geometry	Coordinates	Solutions for	Method	Fluid	References
Bird et al. (1960, 2002)	\parallel	\odot	v_r, T	a	N	[1, 2]
Parnaby and Worth (1974)	V, \parallel	\odot	Δp	a	PL	[3]
Dijksman and Savenije (1985)	V	\S	$v_r, \Delta p$	a	N	Eqs. (4.9) and (4.10) [4]
Kolitawong and Giacomini (2001)	\parallel	$\rightleftharpoons \odot$	v_r	a	N, PL	[5]
Liang (2003)	V	\odot	$v_r, \Delta p$	a	PL	[6]
Kolitawong et al. (2011)	\parallel	$\rightleftharpoons \odot$	T	n	PL	[7]
This paper	V, Λ	\odot	v_r, T	a	N	

a , analytical; n , numerical; N, Newtonian; PL, power-law; T , temperature; V , converging; Λ , diverging; \parallel , straight; v_r , velocity; Δp , pressure drop; $\dot{\gamma}$, shear rate; \odot , cylindrical; \odot , spherical; \S , toroidal; $\rightleftharpoons \odot$, bipolar cylindrical.

Table 2: Dimensional variables.

Variable name	Actual variable	Dimensions	Variable range
Absolute temperature, inner surface	T_0	T	≥ 0
Absolute temperature, initial fluid	T_0	T	≥ 0
Absolute temperature, maximum	T_{\max}	T	≥ 0
Absolute temperature, outer surface	T_0	T	≥ 0
Absolute temperature, rise	T	T	≥ 0
Azimuthal component of gravity	g_ϕ	L/t^2	0
Azimuthal component of heat flux	q_ϕ	M/t^3	0
Azimuthal component of velocity	v_ϕ	L/t	0
Characteristic time, Eq. (90)	$\lambda \equiv \mu / \rho \tilde{C}_p (T_{\max} - T_0)$	t	> 0
Continuity flow function	$C(\theta)$	L^3/t	≤ 0
Density, melt	ρ	M/L^3	≥ 0
Gravity	g	L/t^2	≥ 0
Heat capacity, constant pressure	\tilde{C}_p	$L^2/t^2 T$	≥ 0
Inner spherical radius	r_i	L	≥ 0
Maximum velocity	V_{\max}	L/t	> 0
Outer spherical radius	r_o	L	≥ 0
Pressure	p	M/Lt^2	≥ 0
Pressure drop	$\Delta p \equiv p_o - p_i$	M/Lt^2	≥ 0
Pressure, inner surface	p_i	M/Lt^2	≥ 0
Pressure, outer surface	p_o	M/Lt^2	≥ 0
Radial component in spherical coordinates	r	L	≥ 0
Radial component of gravity	g_r	L/t^2	≤ 0
Radial component of heat flux	q_r	M/t^3	≥ 0
Radial component of velocity	v_r	L/t	\mathbb{R}
Rate of deformation tensor	$\dot{\underline{\gamma}}$	$1/t$	\mathbb{R}^3
Shear rate	$\dot{\gamma}$	$1/t$	\mathbb{R}
Shear stress	τ	M/Lt^2	\mathbb{R}
Shear stress tensor	$\underline{\tau}$	M/Lt^2	\mathbb{R}^3
Spherical polar component of gravity	g_θ	L/t^2	0
Spherical polar component of heat flux	q_θ	M/t^3	\mathbb{R}
Spherical polar component of velocity	v_θ	L/t	0
Time	t	t	≥ 0
Thermal conductivity	k	$ML/t^3 T$	≥ 0
Thermal diffusivity	$\alpha \equiv k / \rho \tilde{C}_p$	L^2/t	≥ 0
Velocity vector	\underline{v}	L/t	\mathbb{R}^3
Viscosity, melt	μ	M/Lt	≥ 0
Volumetric flow rate	Q	L^3/t	≥ 0

L , length; M , mass; T , temperature; t , time.

Where τ_{ij} is the force exerted in the j th direction on a unit area of fluid surface of constant x_i by fluid in the region lesser x_i on fluid in the region greater x_i [2].

Table 3: Dimensionless variables and groups.

Group name	Symbol	Group range
Azimuthal angular coordinate	ϕ	$[0; 2\pi]$
Dimensionless continuity constant, Eq. (63)	$\mathcal{C} \equiv \frac{C\mu}{\Delta p r_i^3}$	\mathbb{R}
Dimensionless continuity constant	$\mathbb{C} \equiv \frac{C\lambda}{r_o^3}$	\mathbb{R}
Dimensionless flow rate, Eq. (3) [3]	$\Omega \equiv \frac{1}{6} \left(1 + \frac{\tan\theta_i}{\tan\theta_o} \right) \left(1 - \frac{\tan\theta_i}{\tan\theta_o} \right)^3$	\mathbb{R}
Function of ξ	B, B_1	\mathbb{R}
Function of θ , Eqs. (32), (33), (54)	a, b, A	\mathbb{R}
Functions of θ_i and θ_o , Eqs. (37), (38), (39), (40)	a_o, a_p, b_o, b_i	\mathbb{R}
Half conical angle, maximum	θ_c	$[\theta_i; \theta_o]$
Half conical angle, inside	θ_i	$\left[0; \frac{\pi}{2} \right]; \theta_o > \theta_i$
Half conical angle, maximum temperature	$\theta_{\max, T}$	$[\theta_i; \theta_o]$
Half conical angle, maximum velocity	$\theta_{\max, v}$	$[\theta_i; \theta_o]$
Half conical angle, minimum velocity	$\theta_{\min, v}$	$[\theta_i; \theta_o]$
Half conical angle, outside	θ_o	$\left[0; \frac{\pi}{2} \right]; \theta_o > \theta_i$
Péclet number, Eq. (92)	$\text{Pe} \equiv \frac{\alpha\lambda(r_o - r_i)}{r_o^3}$	\mathbb{R}
Pressure, Eq. (68)	$\mathcal{P} \equiv \frac{p - p_i}{\Delta p}$	$[0; 1]$
Pressure drop	$\Delta \mathcal{P} \equiv \frac{\Delta p r_i}{\mu V_{\max}}$	\mathbb{R}
Radial position, Eq. (65)	$\mathcal{R} \equiv \frac{r - r_i}{r_o - r_i}$	$[0; 1]$
Pressure to viscosity dimensionless number	$\mathcal{P} \equiv \frac{2\lambda\Delta p}{\mu}$	\mathbb{R}
Reynolds number, Eq. (130)	$\text{Re} \equiv \frac{\rho V_{\max} r_i}{\mu}$	> 0
Shape factors, Eqs. (73), (74), (6), (70)	f_c^o, f_c^i, f_l, f_s	\mathbb{R}
Spherical angular position, Eq. (56)	$\xi \equiv \frac{\theta - \theta_i}{\theta_o - \theta_i}$	$[0; 1]$
Spherical polar angular coordinate	θ	$\left[0; \frac{\pi}{2} \right]$
Spherical radii ratio, Eq. (2)	$\kappa \equiv r_i / r_o$	≥ 0
Temperature	$\Theta \equiv \frac{T - T_0}{T_{\max} - T_0}$	$[0; 1]$
Velocity, Eq. (67)	$\mathcal{V} \equiv \frac{v_r \mu r_o^2}{(p_o - p_i) r_i^3}$	\mathbb{R}
Volumetric flow rate	$\mathcal{Q} \equiv \frac{Q}{V_{\max} r_i^2}$	\mathbb{R}

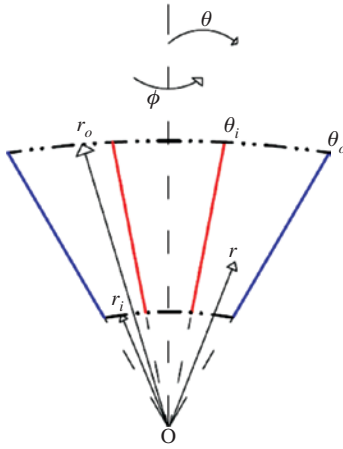


Figure 1: Spherical coordinates for pressure-driven flow through converging coapical concentric conical annulus ($\kappa = \frac{5}{13}$, $\theta_i = 11^\circ$, $\theta_o = 31^\circ$).

Dijksman and Savenije [4] used the special toroidal coordinates to find exact analytical solutions for converging and diverging *non-coapical* and coaxial annular Newtonian flow. By *non-coapical*, we mean that the conical walls do not share the same apex. They even rewrote the equations of continuity and motion in toroidal coordinates (see Appendices I and II of [4]). For coapical converging Newtonian flows, their equation for the velocity (Eq. (4.9) of [4]), rewritten in spherical coordinates, defined in Figure 1 and Table 2 is:

$$v_r = \frac{-3Q(\theta - \theta_i)(\theta - \theta_i - \theta_o)}{\pi r^2 \theta^3 \sin \theta_i} \quad (4)$$

However, Eq. (4) does not satisfy the boundary condition at θ_o given by Eq. (34). Hence, Eqs. (4.9) and (4.10) of [4] should not be used.

Liang [6] also reached analytical solutions for converging annular flow of power-law fluids. For our case, the Liang exact analytical solution written using the variables defined in Figure 1 and Table 2 is:

$$\Delta p = \frac{Q\mu}{3\pi r_i^3 f_L} (1 - \kappa^3) \quad (5)$$

where κ is defined in Eq. (2) and:

$$f_L = \frac{1}{2} \left[(\theta_c - \theta_i)^3 \sin \theta_i + (\theta_o - \theta_c)^3 \sin \theta_o - \frac{1}{2} (\theta_o - \theta_i)^2 (\cos \theta_i - \cos \theta_o) \right] \quad (6)$$

where $\theta [=]$ rad, and in which $\theta_c = \frac{1}{2}(\theta_i + \theta_o)$ for both $u_r(r, \theta_i) = 0$ and $u_r(r, \theta_o) = 0$.

In this work, we use spherical coordinates to analyze viscous dissipation in pressure-driven flow through a verging annular plastics extrusion die. We find exact analytical solutions for the steady state velocity and temperature rise profiles.

2 Materials and methods

We consider molten Newtonian plastics, flowing through verging conical annular dies. Figure 1 shows these annuli, between two coaxial coapical cones. Our analysis follows the transport phenomena approach. We explore the analytical solution for the velocity profile, and then use this to calculate the temperature rise caused by viscous dissipation.

3 Analysis

3.1 Velocity profile

3.1.1 Physical intuition

Figures 2 and 3 show that the molten plastic moves in the r -direction only:

$$v_\theta = v_\phi = 0 \quad (7)$$

where:

$$\underline{v} = (v_r(r, \theta), 0, 0); v_r(r, \theta) \leq 0 \quad (8)$$

for converging flows, and:

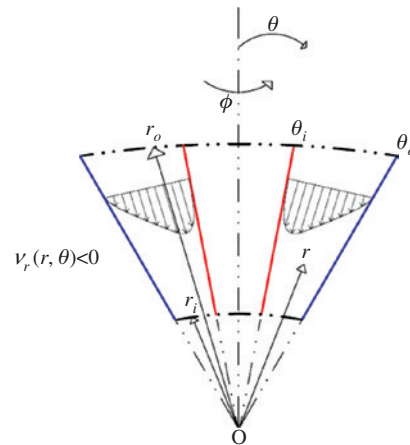


Figure 2: Velocity profile for pressure-driven flow through converging coapical concentric conical annulus ($\kappa = \frac{5}{13}$, $\theta_i = 11^\circ$, $\theta_o = 31^\circ$).

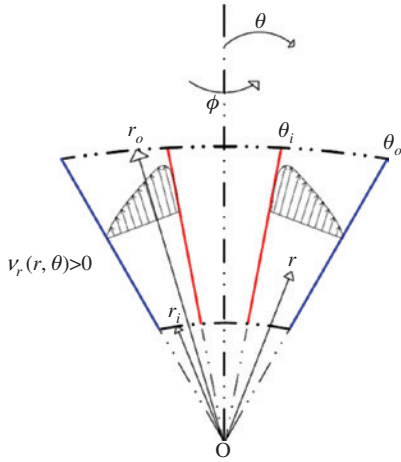


Figure 3: Velocity profile for pressure-driven flow through diverging coapical concentric conical annulus ($\kappa = \frac{5}{13}$, $\theta_i = 11^\circ$, $\theta_o = 31^\circ$).

$$\underline{v} = (v_r(r, \theta), 0, 0); v_r(r, \theta) \geq 0 \tag{9}$$

for diverging flows.

3.1.2 Equation of continuity in spherical coordinates (r, θ, ϕ)

From the equation of continuity (Eq. B.4-3 of [2]), for constant density and using Eq. (7) we get:

$$v_r = \frac{C(\theta)}{r^2} \tag{10}$$

and differentiating gives:

$$\frac{\partial v_r}{\partial r} = \frac{-2C(\theta)}{r^3} \tag{11}$$

which we will use to simplify the rr -component of the rate of deformation tensor, and also, to simplify the r -component of the equation of motion.

3.1.3 Equations of motion in spherical coordinates (r, θ, ϕ)

The r -component of the equation of motion (Eq. B.5-7 of [2]), after applying Eq. (7) and ϕ symmetry, reduces to:

$$\rho v_r \frac{\partial v_r}{\partial r} = \frac{-\partial p}{\partial r} \left[\frac{1}{r^2} \frac{\partial}{\partial r} (r^2 \tau_{rr}) + \frac{1}{r \sin \theta} \frac{\partial}{\partial \theta} (\tau_{\theta r} \sin \theta) - \frac{\tau_{\theta\theta} + \tau_{\phi\phi}}{r} \right] - \rho g \cos \theta \tag{12}$$

Each relevant component of the rate of deformation tensor (§B.1 of [2]), simplified with Eqs. (8), (9), (10) or (11) then gives:

$$\dot{\gamma}_{rr} = 2 \frac{\partial v_r}{\partial r} = \frac{-4C}{r^3} \tag{13}$$

$$\dot{\gamma}_{\theta\theta} = 2 \left(\frac{1}{r} \frac{\partial v_\theta}{\partial \theta} + \frac{v_r}{r} \right) = 2 \frac{v_r}{r} = \frac{2C}{r^3}$$

$$\dot{\gamma}_{\phi\phi} = 2 \left(\frac{1}{r \sin \theta} \frac{\partial v_\phi}{\partial \phi} + \frac{v_r}{r} + \frac{v_\theta \cot \theta}{r} \right) = 2 \frac{v_r}{r} = \Delta_{\theta\theta}$$

$$\dot{\gamma}_{r\theta} = r \frac{\partial}{\partial r} \left(\frac{v_\theta}{r} \right) + \frac{1}{r} \frac{\partial v_r}{\partial \theta} = \frac{1}{r} \frac{\partial v_r}{\partial \theta} = \frac{1}{r} \frac{\partial}{\partial \theta} \left[\frac{C(\theta)}{r^2} \right] = \frac{1}{r^3} \frac{\partial C}{\partial \theta} \tag{14}$$

Hence $\tau_{\theta\theta} = \tau_{\phi\phi}$, so that combining Eq. (12) with Eqs. (10) and (11) yields:

$$-2\rho \frac{C^2}{r^5} = \frac{-\partial p}{\partial r} \left[\frac{1}{r^2} \frac{\partial}{\partial r} (r^2 \tau_{rr}) + \frac{1}{r \sin \theta} \frac{\partial}{\partial \theta} (\tau_{\theta r} \sin \theta) - \frac{2}{r} \tau_{\theta\theta} \right] - \rho g \cos \theta \tag{15}$$

3.1.4 Eliminating stresses

Combining Eqs. (13) and (14) with the constitutive equation for Newtonian fluids:

$$\underline{\underline{\tau}} = -\mu \underline{\underline{\dot{\gamma}}} \tag{16}$$

yields:

$$\tau_{rr} = \frac{4\mu C}{r^3}$$

$$\tau_{\theta\theta} = -\frac{2\mu C}{r^3}$$

$$\tau_{r\theta} = -\frac{\mu}{r^3} \frac{\partial C}{\partial \theta} \tag{17}$$

We can eliminate the stresses from Eq. (15), and since C depends on θ only:

$$-2\rho \frac{C^2}{r^5} = \frac{-\partial p}{\partial r} + \frac{\mu}{r^4 \sin \theta} \frac{d}{d\theta} \left(\frac{dC}{d\theta} \sin \theta \right) - \rho g \cos \theta \tag{18}$$

Neglecting both fluid inertia and gravity we get:

$$0 = \frac{-dp}{dr} + \frac{\mu}{r^4 \sin \theta} \frac{d}{d\theta} \left(\frac{dC}{d\theta} \sin \theta \right) \tag{19}$$

for which the variables easily separate:

$$r^4 \frac{dp}{dr} = \frac{\mu}{\sin \theta} \frac{d}{d\theta} \left(\frac{dC}{d\theta} \sin \theta \right) \tag{20}$$

and thus:

$$r^4 \frac{dp}{dr} = C_1 \tag{21}$$

which is easily integrated to give the (nonlinear) pressure profile:

$$p=C_4-\frac{C_1}{3r^3} \tag{22}$$

from which we learn that the pressure depends at most on r , and which is subject to the pressure boundary conditions:

$$p_o=C_4-\frac{C_1}{3r_o^3} \tag{23}$$

$$p_i=C_4-\frac{C_1}{3r_i^3} \tag{24}$$

where, for converging flows, the outer pressure must exceed the inner:

$$p_o > p_i \tag{25}$$

and for diverging:

$$p_i > p_o \tag{26}$$

Solving Eqs. (23) and (24):

$$C_1=\frac{3(p_o-p_i)r_i^3}{1-\kappa^3} \tag{27}$$

$$C_4=\frac{p_o-\kappa^3 p_i}{1-\kappa^3} \tag{28}$$

where κ is defined in Eq. (2). Hence:

$$p=\frac{1}{1-\kappa^3}\left[p_o-\kappa^3 p_i-\frac{(p_o-p_i)r_i^3}{r^3}\right] \tag{29}$$

Returning to the right side of Eq. (20) gives:

$$\frac{d^2C}{d\theta^2}+\frac{\cos\theta}{\sin\theta}\frac{dC}{d\theta}=\frac{C_1}{\mu} \tag{30}$$

which has the general real solution:

$$C=\frac{-C_1}{2\mu}(a+b)-C_2(a-b)+C_3 \tag{31}$$

where:

$$a\equiv\log(1+\cos\theta) \tag{32}$$

$$b\equiv\log(1-\cos\theta) \tag{33}$$

and where $C[=]C_2[=]C_3[=]C_1/\mu[=]L^3/t$.

Eq. (31) is subject to the no-slip boundary conditions:

$$C(\theta_i)=C(\theta_o)=0 \tag{34}$$

and hence:

$$0=\frac{-C_1}{\mu}(a_o+b_o)-2C_2(a_o-b_o)+2C_3 \tag{35}$$

$$0=\frac{-C_1}{\mu}(a_i+b_i)-2C_2(a_i-b_i)+2C_3 \tag{36}$$

where C_1 is given by Eq. (27), and where:

$$a_o\equiv\log(1+\cos\theta_o) \tag{37}$$

$$b_o\equiv\log(1-\cos\theta_o) \tag{38}$$

$$a_i\equiv\log(1+\cos\theta_i) \tag{39}$$

$$b_i\equiv\log(1-\cos\theta_i) \tag{40}$$

Solving Eqs. (35) and (36) and substituting the results into Eq. (31) gives:

$$C=\frac{3(p_o-p_i)r_i^3}{2\mu(1-\kappa^3)}\left[-(a+b)+\left(\frac{a_o+b_o-a_i-b_i}{a_o-b_o-a_i+b_i}\right)(a-b)+2\left(\frac{a_o b_i-a_i b_o}{a_o-b_o-a_i+b_i}\right)\right] \tag{41}$$

Substituting this into Eq. (10) we get the exact solution for the velocity profile in spherical coordinates for pressure-driven flow through conical coapical coaxial annulus:

$$v_r=\frac{3(p_o-p_i)r_i^3}{2\mu(1-\kappa^3)r^2}\left[-(a+b)+\left(\frac{a_o+b_o-a_i-b_i}{a_o-b_o-a_i+b_i}\right)(a-b)+2\left(\frac{a_o b_i-a_i b_o}{a_o-b_o-a_i+b_i}\right)\right] \tag{42}$$

be it converging or diverging. Differentiating Eq. (42) and solving for θ_{\min,v_r} we get:

$$\theta_{\min,v_r}=\arccos\left(\frac{-a_o-b_o+a_i+b_i}{a_o-b_o-a_i+b_i}\right) \tag{43}$$

For converging (and diverging) flows, $\theta_{\min,v_r} < (\theta_i + \theta_o) / 2$, with $\theta_i, \theta_o \in [0; \pi/2]$, and thus the minimum (and maximum) velocity cones are nearer the inner surface than the outer. This is why shear rates $\dot{\gamma}_{r\theta}$ (and thus the shear stresses $\tau_{r\theta}$) on the inner cone are higher than on the outer (for both converging and diverging flows).

We now turn our attention to the ϕ -component of the equation of motion (Eq. B.5-9 of [2]) which, following Subsections 3.1.3 and 3.1.4, and since we are neglecting gravity, gives:

$$\begin{aligned} & \rho \left(\frac{\partial v_\phi}{\partial t} + v_r \frac{\partial v_\phi}{\partial r} + \frac{v_\theta}{r} \frac{\partial v_\phi}{\partial \theta} + \frac{v_\phi}{r \sin \theta} \frac{\partial v_\phi}{\partial \phi} + \frac{v_r v_r + v_\theta v_\theta \cot \theta}{r} \right) \\ &= \frac{-1}{r \sin \theta} \frac{\partial p}{\partial \phi} \left[\frac{1}{r^3} \frac{\partial}{\partial r} (r^3 \tau_{r\phi}) + \frac{1}{r \sin \theta} \frac{\partial}{\partial \theta} (\tau_{\theta\phi} \sin \theta) \right. \\ & \left. + \frac{1}{r \sin \theta} \frac{\partial \tau_{\phi\phi}}{\partial \phi} + \frac{\tau_{\phi\phi} \cot \theta}{r} \right] \end{aligned} \quad (44)$$

Eliminating the stresses using:

$$\begin{aligned} \tau_{r\phi} &= \tau_{\theta\phi} = 0 \\ \tau_{\phi\phi} &= -\frac{2\mu C}{r^3} \end{aligned} \quad (45)$$

we get,

$$\frac{\partial p}{\partial \phi} = 0 \quad (46)$$

from which we learn that the pressure does not depend on ϕ .

Similarly, for the θ -component (Eq. B.5-8 of [2]), by following Subsections 3.1.3 and 3.1.4 we get:

$$\begin{aligned} & \rho \left(\frac{\partial v_\theta}{\partial t} + v_r \frac{\partial v_\theta}{\partial r} + \frac{v_\theta}{r} \frac{\partial v_\theta}{\partial \theta} + \frac{v_\phi}{r \sin \theta} \frac{\partial v_\theta}{\partial \phi} - \frac{v_r v_\theta - v_\phi^2 \cot \theta}{r} \right) \\ &= \frac{-1}{r} \frac{\partial p}{\partial \theta} \left[\frac{1}{r^3} \frac{\partial}{\partial r} (r^3 \tau_{r\theta}) + \frac{1}{r \sin \theta} \frac{\partial}{\partial \theta} (\tau_{\theta\theta} \sin \theta) \right. \\ & \left. + \frac{1}{r \sin \theta} \frac{\partial \tau_{\phi\theta}}{\partial \phi} - \frac{\tau_{\phi\theta} \cot \theta}{r} \right] \end{aligned} \quad (47)$$

and then using:

$$\begin{aligned} \tau_{\theta\theta} &= \tau_{\phi\theta} = -\frac{2\mu C}{r^3} \\ \tau_{r\theta} &= -\frac{\mu}{r^3} \frac{\partial C}{\partial \theta} \\ \tau_{\phi\theta} &= 0 \end{aligned} \quad (48)$$

to eliminate the stresses gives:

$$\frac{\partial p}{\partial \theta} = \frac{2\mu}{r^3} \frac{dC}{d\theta} \quad (49)$$

and integrating yields:

$$p = \frac{2\mu C}{r^3} + C_5(r) \quad (50)$$

Substituting Eq. (29) into Eq. (50) gives:

$$\frac{1}{1-\kappa^3} \left[p_o - \kappa^3 p_i - \frac{(p_o - p_i) r_i^3}{r^3} \right] = \frac{2\mu C}{r^3} + C_5(r) \quad (51)$$

Solving for C_5 at $\theta = \theta_o$ we get:

$$C_5 = \frac{1}{1-\kappa^3} \left[p_o - \kappa^3 p_i - \frac{(p_o - p_i) r_i^3}{r^3} \right] = p(r) \quad (52)$$

Substituting Eqs. (27), (41) and (52) into Eq. (50) yields the two dimensional nonlinear pressure profile:

$$p(r, \theta) = \frac{(p_o - p_i) r_i^3}{(1-\kappa^3) r^3} (A-1) + \frac{p_o - \kappa^3 p_i}{1-\kappa^3} \quad (53)$$

with:

$$A(\theta) \equiv 3 \left[-(a+b) + \left(\frac{a_o + b_o - a_i - b_i}{a_o - b_o - a_i + b_i} \right) (a-b) + 2 \left(\frac{a_o b_i - a_i b_o}{a_o - b_o - a_i + b_i} \right) \right] \quad (54)$$

For most plastics extrusion die designs:

$$A \ll 1 \quad (55)$$

Therefore Eq. (53) reduces to Eq. (29) and our assumption that p depends on r only (see Subsection 3.1.4) is confirmed.

3.1.5 Nondimensional velocity and pressure

We begin our nondimensionalization by rearranging:

$$\xi \equiv \frac{\theta - \theta_i}{\theta_o - \theta_i} \quad (56)$$

from Table 3, to give:

$$\theta = \xi(\theta_o - \theta_i) + \theta_i \quad (57)$$

which, substituted into Eqs. (32) and (33), yields:

$$a \equiv \log[1 + \cos(\xi(\theta_o - \theta_i) + \theta_i)] \quad (58)$$

$$b \equiv \log[1 - \cos(\xi(\theta_o - \theta_i) + \theta_i)] \quad (59)$$

Next, in Eq. (41), we let:

$$B(\xi, \theta_i, \theta_o) \equiv -(a+b) + \left(\frac{a_o + b_o - a_i - b_i}{a_o - b_o - a_i + b_i} \right) (a-b) + 2 \left(\frac{a_o b_i - a_i b_o}{a_o - b_o - a_i + b_i} \right) \quad (60)$$

so that:

$$C = \frac{BC_1}{2\mu} \quad (61)$$

Substituting Eq. (27) into Eq. (61), we get:

$$C = \frac{3B(p_o - p_i) r_i^3}{2\mu(1-\kappa^3)} \quad (62)$$

Using this with Table 3 gives:

$$\mathcal{C} \equiv \frac{C\mu}{(p_o - p_i)r_i^3} \equiv \frac{3B}{2(1-\kappa^3)} \quad (63)$$

and thus:

$$C = \frac{\mathcal{C}(p_o - p_i)r_i^3}{\mu} \quad (64)$$

which we will use below. Also letting:

$$\mathcal{R} \equiv \frac{r - r_i}{r_o - r_i} = \frac{r - \kappa r_o}{r_o - \kappa r_o} \quad (65)$$

so that:

$$r = r_o [\mathcal{R}(1-\kappa) + \kappa] \quad (66)$$

Substituting Eqs. (64) and (66) into Eq. (10), rearranging, and using Table 3, we get the dimensionless velocity profile:

$$\mathcal{V} \equiv \frac{v_r \mu r_o^2}{(p_o - p_i)r_i^3} = \frac{\mathcal{C}}{[\mathcal{R}(1-\kappa) + \kappa]^2} = \frac{3B(\xi)}{2(1-\kappa^3)[\mathcal{R}(1-\kappa) + \kappa]^2} \quad (67)$$

where κ is defined in Eq. (2).

Using Table 3 with Eq. (29) and rearranging gives the dimensionless pressure profile:

$$\mathcal{P} \equiv \frac{p - p_i}{\Delta p} = \frac{1}{1-\kappa^3} \left[1 - \frac{\kappa^3}{[\mathcal{R}(1-\kappa) + \kappa]^3} \right]; A \ll 1 \quad (68)$$

3.1.6 Nondimensional $\mathcal{Q}/\Delta\mathcal{P}$

Integrating Eq. (42) twice, with respect to θ and ϕ , and then rearranging gives:

$$\Delta p = \frac{Q\mu(1-\kappa^3)}{3\pi r_i^3 f_s} \quad (69)$$

where:

$$\begin{aligned} f_s = & \left(1 - \frac{a_o + b_o - a_i - b_i}{a_o - b_o - a_i + b_i} \right) [a_o(1 + \cos\theta_o) - a_i(1 + \cos\theta_i)] \\ & - \left(1 + \frac{a_o + b_o - a_i - b_i}{a_o - b_o - a_i + b_i} \right) [b_o(1 - \cos\theta_o) - b_i(1 - \cos\theta_i)] \\ & - 2(\cos\theta_o - \cos\theta_i) \left(1 + \frac{a_o b_i - a_i b_o}{a_o - b_o - a_i + b_i} \right) \end{aligned} \quad (70)$$

with a_o, b_o, a_i and b_i defined in Eqs. (37)–(40). Equation (70) is the *first main result* of this paper. Using Tables 2 and 3, we adimensionalize Eq. (69) to get:

$$\frac{1-\kappa^3}{3\pi} \frac{\mathcal{Q}}{\Delta\mathcal{P}} = f_s \quad (71)$$

Figure 10 illustrates Eq. (71) and shows how the dimensionless flow rate per unit pressure drop, f_s , changes with the extrusion die shape, θ_i and θ_o . Practitioners can use Figure 10 to get the volumetric flow rate graphically, or the pressure drop (see worked example in Section 5).

In Figure 11, we will compare the previous approximate solutions of Parnaby and Worth [3] [Eq. (1)] and of Liang [6] [Eq. (5)] with our exact solution [Eq. (71)]. For this, we must nondimensionalize Eqs. (1) and (5) in the same way as our Eq. (71). For Parnaby and Worth [3] [Eq. (1)], we get:

$$f_c^i < \frac{1-\kappa^3}{3\pi} \frac{\mathcal{Q}}{\Delta\mathcal{P}} < f_c^o \quad (72)$$

where:

$$f_c^o \equiv \frac{\Omega \cos^3 \theta_o \tan^4 \theta_o}{2} \quad (73)$$

$$f_c^i \equiv \frac{\Omega \cos^3 \theta_i \tan^4 \theta_i}{2} \quad (74)$$

where Ω is defined in Eq. (3), and for Liang [6] [Eq. (5)], we get:

$$\frac{1-\kappa^3}{3\pi} \frac{\mathcal{Q}}{\Delta\mathcal{P}} = f_L \quad (75)$$

with f_L defined in Eq. (6).

3.2 Temperature rise

In this section, we focus on the temperature rise caused by the viscous dissipation associated with the velocity profile given by our exact solution, Eq. (42). Specifically, we consider melt entering the conical die (illustrated in Figures 1, 4 and 5) at a uniform temperature T_o and with isothermal inner and outer conical surfaces also at T_o . We are, of course, aware that the extrusion die surfaces can be controlled with other thermal boundary conditions. These conditions lie beyond the scope of this work.

3.2.1 Physical intuition

Figures 4 and 5 show how the temperature profile evolves in the dies for converging and diverging flows. When

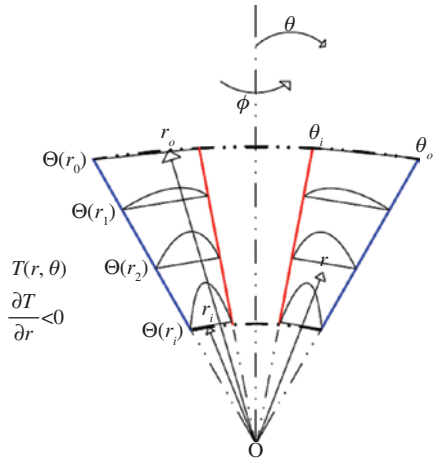


Figure 4: Temperature rise profile for pressure-driven flow through converging coapical concentric conical annulus ($\kappa = \frac{5}{13}$, $\theta_i = 11^\circ$, $\theta_o = 31^\circ$).

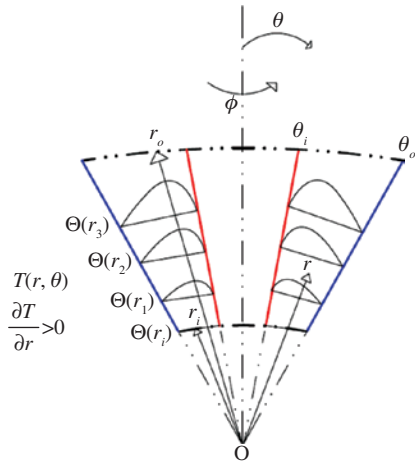


Figure 5: Temperature rise profile for pressure-driven flow through diverging coapical concentric conical annulus ($\kappa = \frac{5}{13}$, $\theta_i = 11^\circ$, $\theta_o = 31^\circ$).

viscous dissipation matters, the temperature rises as the melt flows from r_o to r_i (r_i to r_o) for converging (diverging) flows. Not unlike $v_r(r, \theta)$, the temperature also depends on both r and θ , $T(r, \theta)$. Thus, for converging flows through isothermal die walls we have:

$$\frac{\partial T}{\partial r} < 0 \tag{76}$$

and:

$$T(r_o, \theta) = T(r, \theta_o) = T(r, \theta_i) = T_o \tag{77}$$

whereas for diverging flows we have:

$$\frac{\partial T}{\partial r} > 0 \tag{78}$$

and:

$$T(r_i, \theta) = T(r, \theta_o) = T(r, \theta_i) = T_o \tag{79}$$

For both converging and diverging flows, we define:

$$\left. \frac{\partial T}{\partial \theta} \right|_{T_{\max}(r)} = 0; \theta = \theta_{\max, T}(r) \tag{80}$$

which defines the hottest surface in the flowing melt, which is at most a function of r .

3.2.2 Viscous dissipation term in spherical coordinates (r, θ, ϕ)

We begin by combining the general expression for the viscous dissipation in spherical coordinates (Eq. (C) of Table A.7-3 of [2]) with our physical intuition for the velocity, Eq. (7):

$$\begin{aligned} (\tau : \nabla v) = & \tau_{rr} \left(\frac{\partial v_r}{\partial r} \right) + \tau_{\theta\theta} \left(\frac{v_r}{r} \right) + \tau_{\phi\phi} \left(\frac{v_r}{r} \right) + \tau_{r\theta} \left(\frac{1}{r} \frac{\partial v_r}{\partial \theta} \right) \\ & + \tau_{r\phi} \left(\frac{1}{r \sin \theta} \frac{\partial v_r}{\partial \phi} \right) \end{aligned} \tag{81}$$

which when combined with the velocity profile and its derivative, Eqs. (10) and (11), gives:

$$(\tau : \nabla v) = \tau_{rr} \left(\frac{\partial v_r}{\partial r} \right) + \tau_{\theta\theta} \left(\frac{v_r}{r} \right) + \tau_{\phi\phi} \left(\frac{v_r}{r} \right) + \tau_{r\theta} \left(\frac{1}{r} \frac{\partial v_r}{\partial \theta} \right) \tag{82}$$

from which we eliminate the stresses using Eqs. (17), (45), $\tau_{rr} = -2\tau_{\theta\theta}$ and $\tau_{\phi\phi} = \tau_{\theta\theta}$ to get:

$$(\tau : \nabla v) = \frac{-\mu}{r^6} \left[12C^2 + \left(\frac{dC}{d\theta} \right)^2 \right] \tag{83}$$

which we will use in Subsection 3.2.3, and where the exact solution for C is given by Eq. (41).

3.2.3 Equation of energy in spherical coordinates (r, θ, ϕ)

We begin by simplifying the equation of energy written in terms of temperature for an incompressible fluid (Eq. B.8-3 of [2]), with ϕ symmetry for the longitudinal heat flux, q_ϕ , gives:

$$\rho \hat{C}_p v_r \frac{\partial T}{\partial r} = - \left[\frac{1}{r^2} \frac{\partial}{\partial r} (r^2 q_r) + \frac{1}{r \sin \theta} \frac{\partial}{\partial \theta} (q_\theta \sin \theta) \right] - (\tau : \nabla v) \tag{84}$$

Eliminating the heat fluxes using Fourier's law (Eqs. B.2-7 and B.2-8 of [2]) we get:

$$\rho \hat{C}_p v_r \frac{\partial T}{\partial r} = k \left[\frac{1}{r^2} \frac{\partial}{\partial r} \left(r^2 \frac{\partial T}{\partial r} \right) + \frac{1}{r \sin \theta} \frac{\partial}{\partial \theta} \left(\frac{1}{r} \frac{\partial T}{\partial \theta} \sin \theta \right) \right] - (\tau : \nabla v) \quad (85)$$

Now, if we assume that axial conduction is negligible (with respect to radial convection):

$$\rho \hat{C}_p v_r \frac{\partial T}{\partial r} \gg k \frac{1}{r^2} \frac{\partial}{\partial r} \left(r^2 \frac{\partial T}{\partial r} \right) \quad (86)$$

then:

$$v_r \frac{\partial T}{\partial r} = \frac{\alpha}{r \sin \theta} \frac{\partial}{\partial \theta} \left(\frac{1}{r} \frac{\partial T}{\partial \theta} \sin \theta \right) - \frac{1}{\rho \hat{C}_p} (\tau : \nabla v) \quad (87)$$

where $\alpha \equiv k / \rho \hat{C}_p$ is the thermal diffusivity (see Table 2). Substituting Eqs. (10) and (83) into (87) and rearranging gives:

$$C \frac{\partial T}{\partial r} = \frac{\alpha}{\sin \theta} \frac{\partial}{\partial \theta} \left(\sin \theta \frac{\partial T}{\partial \theta} \right) + \frac{1}{\rho \hat{C}_p} \frac{\mu}{r^4} \left[12C^2 + \left(\frac{dC}{d\theta} \right)^2 \right] \quad (88)$$

which is subject to the boundary conditions given by Eqs. (77) and (79).

3.2.4 Dimensionless temperature rise

Using Tables 2 and 3, we rewrite Eq. (88) as:

$$\frac{\partial \Theta}{\partial \mathcal{R}} = \frac{\alpha r_o (1-\kappa)}{C \sin \theta} \frac{\partial}{\partial \theta} \left(\sin \theta \frac{\partial \Theta}{\partial \theta} \right) + \left[\frac{\mu}{\rho \hat{C}_p (T_{\max} - T_0)} \right] \frac{(1-\kappa)}{r_o^3 [\mathcal{R}(1-\kappa) + \kappa]^4} \left[12C + \frac{1}{C} \left(\frac{dC}{d\theta} \right)^2 \right] \quad (89)$$

which uncovers the characteristic time:

$$\lambda \equiv \frac{\mu}{\rho \hat{C}_p (T_{\max} - T_0)} \quad (90)$$

so that:

$$\frac{\partial \Theta}{\partial \mathcal{R}} = \frac{\text{Pé}}{C \sin \theta} \frac{\partial}{\partial \theta} \left(\sin \theta \frac{\partial \Theta}{\partial \theta} \right) + \frac{\lambda (1-\kappa)}{r_o^3 [\mathcal{R}(1-\kappa) + \kappa]^4} \left[12C + \frac{1}{C} \left(\frac{dC}{d\theta} \right)^2 \right] \quad (91)$$

where we have also uncovered the Péclet number:

$$\text{Pé} \equiv \frac{\alpha \lambda (r_o - r_i)}{r_o^3} \quad (92)$$

Further, using Table 3, yields:

$$\frac{\partial \Theta}{\partial \mathcal{R}} = \frac{\text{Pé}}{C \sin \theta} \frac{\partial}{\partial \theta} \left(\sin \theta \frac{\partial \Theta}{\partial \theta} \right) + \frac{1-\kappa}{[\mathcal{R}(1-\kappa) + \kappa]^4} \left[12C + \frac{1}{C} \left(\frac{dC}{d\theta} \right)^2 \right] \quad (93)$$

which we will use presently.

In this Subsection, we begin by neglecting conduction in the θ -direction, and finish with an exact analytical solution for the temperature rise that is consistent with isothermal, inner and outer die walls, Eqs. (77) and (79). Neglecting conduction in the θ -direction ($\text{Pé} \ll 1$), Eq. (93) reduces to:

$$\frac{\partial \Theta}{\partial \mathcal{R}} = \frac{1-\kappa}{[\mathcal{R}(1-\kappa) + \kappa]^4} \left[12C + \frac{1}{C} \left(\frac{dC}{d\theta} \right)^2 \right] \quad (94)$$

and has the exact solution:

$$\Theta = C_6 \cdot \frac{1}{3[\mathcal{R}(1-\kappa) + \kappa]^3} \left[12C + \frac{1}{C} \left(\frac{dC}{d\theta} \right)^2 \right] \quad (95)$$

subject to the entrance condition, which for converging flows is:

$$\Theta(\mathcal{R}_o) = \Theta \left(\frac{r_o - r_i}{r_o - r_i} \right) = \Theta(1) = 0 \quad (96)$$

so that:

$$\Theta = \left[1 - \frac{1}{[\mathcal{R}(1-\kappa) + \kappa]^3} \right] \left[4C + \frac{1}{3C} \left(\frac{dC}{d\theta} \right)^2 \right] \quad (97)$$

and for diverging flows is:

$$\Theta(\mathcal{R}_i) = \Theta \left(\frac{r_i - r_i}{r_o - r_i} \right) = \Theta(0) = 0 \quad (98)$$

so that:

$$\Theta = \left[\frac{1}{\kappa^3} - \frac{1}{[\mathcal{R}(1-\kappa) + \kappa]^3} \right] \left[4C + \frac{1}{3C} \left(\frac{dC}{d\theta} \right)^2 \right] \quad (99)$$

Using Eq. (133), proven in Appendix 7.2, we get:

$$\left(\frac{d\Theta}{d\xi} \right)^2 = \left(\frac{dC}{d\theta} \right)^2 = 0; A^2 \ll 1 \quad (100)$$

which, when applied to Eqs. (97) and (99) gives:

$$\Theta = 4C \left[1 - \frac{1}{[\mathcal{R}(1-\kappa) + \kappa]^3} \right]; A^2 \ll 1 \quad (101)$$

$$\Theta = 4C \left[\frac{1}{\kappa^3} - \frac{1}{[\mathcal{R}(1-\kappa) + \kappa]^3} \right]; A^2 \ll 1 \quad (102)$$

where the condition $A \ll 1$ [Eqs. (54) and (55)] on our pressure and velocity [Eqs. (29) and (42)], upon which Eqs. (101) and (102) are based, is already sufficient for $A^2 \ll 1$. The reader is reminded that, for most plastics extrusion die designs, $A \ll 1$.

Since $\mathbb{C}(\theta_o) = \mathbb{C}(\theta_i) = 0$, the temperature rise on the die surfaces is also zero, $\Theta(\theta_o) = \Theta(\theta_i) = 0$. In other words, Eqs. (101) and (102) are exactly consistent with the isothermal wall boundary conditions Eqs. (77) and (79), which we have yet to use.

Using Table 3, Eqs (101) and (102) become:

$$\Theta = \left[\frac{2\lambda(p_o - p_i)\kappa^3}{\mu(1-\kappa^3)} \right] \left[1 - \frac{1}{[\mathcal{R}(1-\kappa) + \kappa]^3} \right] A \quad (103)$$

$$\Theta = \left[\frac{2\lambda(p_o - p_i)\kappa^3}{\mu(1-\kappa^3)} \right] \left[\frac{1}{\kappa^3} - \frac{1}{[\mathcal{R}(1-\kappa) + \kappa]^3} \right] A \quad (104)$$

with A already defined in Eq. (54). We next differentiate Eqs. (103) and (104) to get the hottest surface in the flowing melt:

$$\theta_{\max, T} = \arccos \left(\frac{-a_o - b_o + a_i + b_i}{a_o - b_o - a_i + b_i} \right) \quad (105)$$

which is conical, and which matches the velocity minimum cone, $\theta = \theta_{\min, v}$, given by Eq. (43). We thus find that the temperature maximum cone $\theta = \theta_{\max, T}$ is nearer the inner surface than the outer.

Using Table 3 to rewrite Eqs. (103) and (104) we get:

$$\Theta(\mathcal{R}, \xi) = \mathbb{P} \left(\frac{\kappa^3}{1-\kappa^3} \right) \left[1 - \frac{1}{[\mathcal{R}(1-\kappa) + \kappa]^3} \right] B_1 \quad (106)$$

$$\Theta(\mathcal{R}, \xi) = \mathbb{P} \left(\frac{\kappa^3}{1-\kappa^3} \right) \left[\frac{1}{\kappa^3} - \frac{1}{[\mathcal{R}(1-\kappa) + \kappa]^3} \right] B_1 \quad (107)$$

Eqs. (106) and (107) give the nondimensional temperature rise for converging and diverging flows, respectively, and these are thus the *second main result* of this work. Equations (106) and (107) are exactly consistent with the isothermal wall boundary conditions Eqs. (77) and (79). In Section 4, we will differentiate Eqs. (106) and (107) to calculate the corresponding cooling requirement for conical die surfaces.

4 Results and discussion

In this section, we will illustrate and discuss the main results of our analysis in Section 3. We graph the velocity

and then the temperature profiles for a specific die design: $\theta_i = 10^\circ$, $\theta_o = 15^\circ$ and $\kappa = \frac{1}{5}$. We further compare our exact

solution [Eq. (71)] for the throughput per unit pressure drop with prior approximations of Parnaby and Worth [3] [Eq. (72)] and of Liang [6] [Eq. (75)]. We will close Section 4 with a dimensionless graph for Eq. (71) that is specifically for practitioners of plastic pipe extrusion die design.

4.1 Velocity profile

In the next two subsections, we discuss Figures 6 and 7, which illustrate the velocity profiles for converging and diverging dies.

4.1.1 Converging flows

The accelerating velocity for converging die flows is negative, and the pressure drop in Eq. (42), is positive. Figure 6 illustrates the velocity profile shape for a particular converging die design. We see that the minimum velocity cone is nearer the inner surface. Using Eq. (43) for the specific die considered, this minimum velocity cone is $\theta_{\min, v} \approx 12.42^\circ$, which is just inside the midcone, $\theta = 12.5^\circ$.

4.1.2 Diverging flows

The decelerating velocity for diverging die flows is positive, and the pressure drop in Eq. (42) is negative. Figure 7

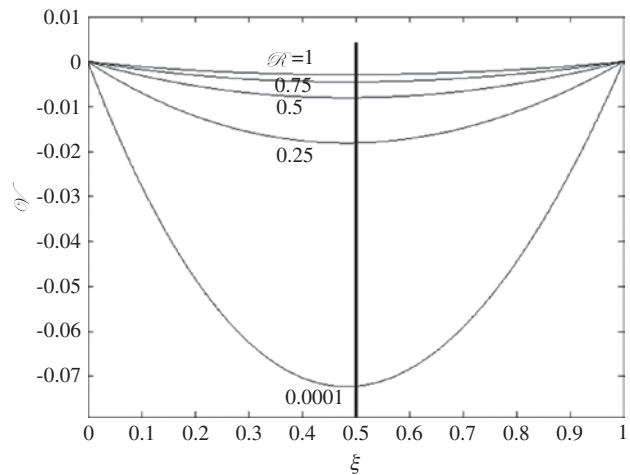


Figure 6: Dimensionless velocity profile [Eq. (67)] for pressure-driven flow through converging coapical concentric conical annulus for different dimensionless conical half angles and dimensionless radial positions ($\kappa = \frac{1}{5}$, $\theta_i = 10^\circ$, $\theta_o = 15^\circ$).

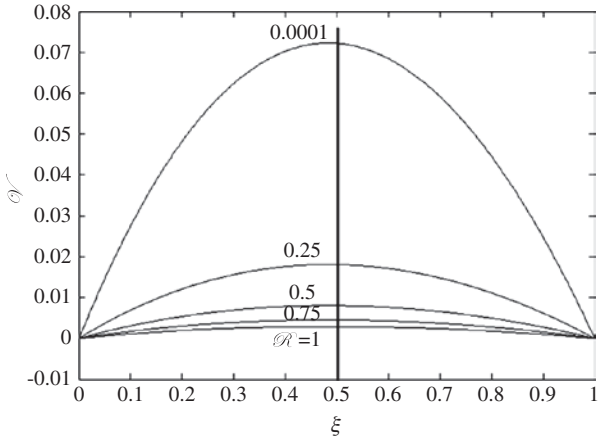


Figure 7: Dimensionless velocity profile [Eq. (67)] for pressure-driven flow through diverging coapical concentric conical annulus for different dimensionless conical half angles and dimensionless radial positions ($\kappa = \frac{1}{5}$, $\theta_i = 10^\circ$, $\theta_o = 15^\circ$).

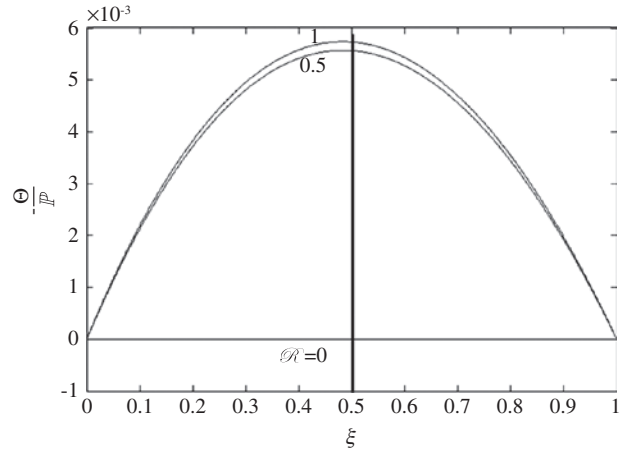


Figure 9: Dimensionless temperature rise profile [Eq. (107)] for pressure-driven flow through diverging coapical concentric conical annulus for different dimensionless conical half angles and dimensionless radial positions ($\kappa = \frac{1}{5}$, $\theta_i = 10^\circ$, $\theta_o = 15^\circ$).

illustrates the velocity profile shape for a specific diverging die design. We see that the maximum velocity cone is nearer the inner surface. Using Eq. (43) for the specific die considered, this maximum velocity cone is $\theta_{\max,v} \approx 12.42^\circ$, which is just inside the midcone, $\theta = 12.5^\circ$.

4.2 Temperature rise profile

In the following two subsections, we discuss Figures 8 and 9, which illustrate the temperature rise profiles in the converging and diverging dies.

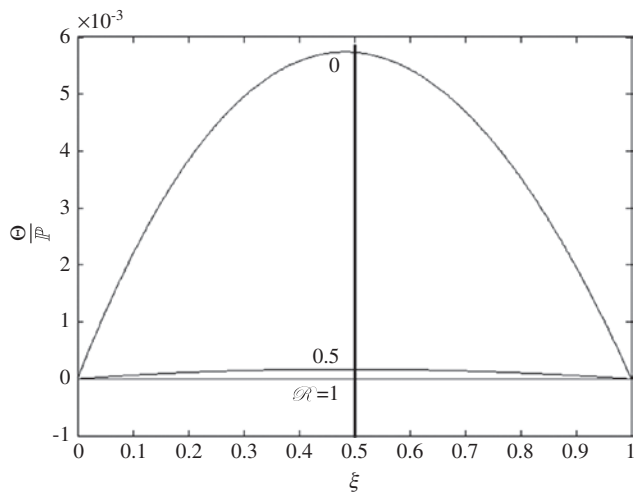


Figure 8: Dimensionless temperature rise profile [Eq. (106)] for pressure-driven flow through converging coapical concentric conical annulus for different dimensionless conical half angles and dimensionless radial positions ($\kappa = \frac{1}{5}$, $\theta_i = 10^\circ$, $\theta_o = 15^\circ$).

4.2.1 Converging flows

In Figure 8, we plot the dimensionless temperature rise per unit pressure drop, $\Theta(\mathcal{R}, \xi)/\mathbb{P}$ which shows the shape of the temperature rise for a specific converging die design. The surface of maximum temperature rise is conical $\theta_{\max,T} = \theta_{\min,v} \approx 12.42^\circ$, which matches the minimum velocity cone. Figure 8 also shows that the wall temperatures are constant at T_0 and thus the walls are isothermal. To achieve this condition, to compensate for viscous heating, the walls must be cooled.

The expression for the required heat flux for cooling is given by (Eq. B.2-8 of [2]):

$$q_\theta = -k \frac{1}{r} \frac{\partial T}{\partial \theta} \tag{108}$$

Substituting Eq. (106), into Eq. (108), and evaluating the result for the inner surface gives the cooling load requirement:

$$q_{\theta_i} = \frac{4k\Delta p\kappa^3}{\rho\tilde{C}_p(1-\kappa^3)\sin\theta_i} \left(\frac{1}{r} \frac{r_o^3}{r^4} \right) \left(\cos\theta_i + \frac{a_o + b_o - a_i - b_i}{a_o - b_o - a_i + b_i} \right) \tag{109}$$

and for the outer surface:

$$q_{\theta_o} = \frac{4k\Delta p\kappa^3}{\rho\tilde{C}_p(1-\kappa^3)\sin\theta_o} \left(\frac{1}{r} \frac{r_o^3}{r^4} \right) \left(\cos\theta_o + \frac{a_o + b_o - a_i - b_i}{a_o - b_o - a_i + b_i} \right) \tag{110}$$

From Eqs. (109) and (110), we conclude that the cooling load at the inner die cone must be higher than for the outer.

4.2.2 Diverging flows

In Figure 9, we plot the dimensionless temperature rise per unit pressure drop, $-\Theta(\mathcal{R}, \xi)/\mathbb{P}$, which shows the shape of the temperature rise for a specific diverging die design. The surface of maximum temperature rise is conical $\theta_{\max,T} = \theta_{\max,v_r} \approx 12.42^\circ$, which matches the maximum velocity cone. Figure 9 also shows that the wall temperatures are constant at T_0 and thus the walls are isothermal. To achieve this condition, to compensate for viscous heating, the walls must be cooled.

Substituting Eq. (107), into Eq. (108), and evaluating the result for the inner surface gives the cooling load requirement:

$$q_{\theta_i} = \frac{4k\Delta p\kappa^3}{\rho\tilde{C}_p(1-\kappa^3)\sin\theta_i} \left(\frac{1}{r\kappa^3} - \frac{r_o^3}{r^4} \right) \left(\cos\theta_i + \frac{a_o+b_o-a_i-b_i}{a_o-b_o-a_i+b_i} \right) \quad (111)$$

and for the outer surface:

$$q_{\theta_o} = \frac{4k\Delta p\kappa^3}{\rho\tilde{C}_p(1-\kappa^3)\sin\theta_o} \left(\frac{1}{r\kappa^3} - \frac{r_o^3}{r^4} \right) \left(\cos\theta_o + \frac{a_o+b_o-a_i-b_i}{a_o-b_o-a_i+b_i} \right) \quad (112)$$

From Eqs. (111) and (112), we conclude that the cooling at the inner die cone must be higher than for the outer.

4.3 Throughput per unit pressure drop

In this section, we use Figure 10 to compare our exact solution [Eq. (71)] for the throughput per unit pressure drop with prior approximations of Parnaby and Worth [3]

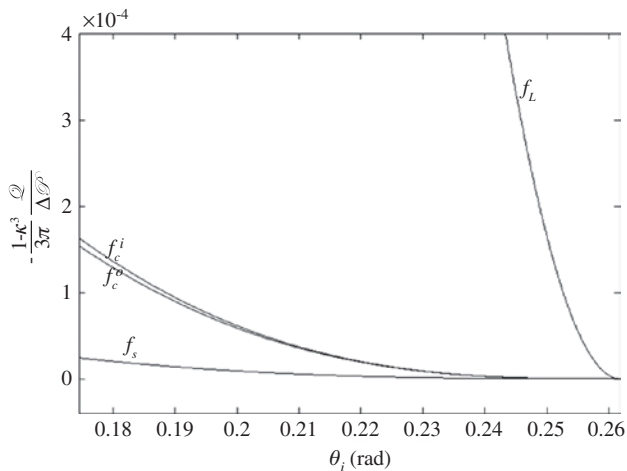


Figure 10: Shape factors (dimensionless volumetric flow rate), f_s [Eq. (71)], (f_c^i, f_c^o) [Eq. (72)], f_L [Eq. (75)], vs. θ_i in radians and parameterized with $\theta_o = 15^\circ = \pi/12$ rad.

[Eq. (72)] and of Liang [6] [Eq. (75)]. Figure 10 has been constructed for: $110^\circ \leq \theta_i \leq 15^\circ$, $\theta_o = 15^\circ$ and $\kappa = \frac{1}{5}$, which includes the special basis $\theta_i = 10^\circ$, $\theta_o = 15^\circ$ and $\kappa = \frac{1}{5}$ that we used for Figures 6–9. For these conditions, Figure 10 shows that whereas the cylindrical approximation of Parnaby and Worth [3] [Eq. (72)] slightly overpredicts the flow rate, Liang [6] [Eq. (75)] grossly overpredicts. Figure 11 charts the flow rate per unit pressure drop predicted by our exact solution, Eq. (71). We provide this dimensionless graph specifically for plastic pipe extrusion die designers. We will use Figure 11 presently.

5 Worked example

An engineer gathers the following process details for her polycarbonate pipe extrusion line, and specifically for the converging connection between her extruder and her straight annular die land: $\theta_o = 31.0^\circ$, $\theta_i = 11.0^\circ$, $r_o = 0.130$ m and $r_i = 0.0500$ m, with the throughput of $\rho Q = -0.0100$ kg/s, and the material properties at the operating temperature are $\mu = 1.10 \times 10^7$ Pa·s, $\rho = 900$ kg/m³, $\tilde{C}_p = 1.60 \times 10^3$ J/kg·°C and $k = 0.1$ W/m.

She wants to estimate (i) the required pressure drop for the given throughput and (ii) the temperature rise in the die.

(i) Using Eq. (54), she first gets $A(\theta_{\min,v_r}) = A(20.2^\circ) = -0.0941$ which satisfies Eq. (55). She then interpolates Figure 11 with $\cos\theta_i = 0.982$ and $\cos\theta_o = 0.857$ to get, for our exact solution:

$$f_s \approx -10^{-2.59} \approx -0.00257 \quad (113)$$

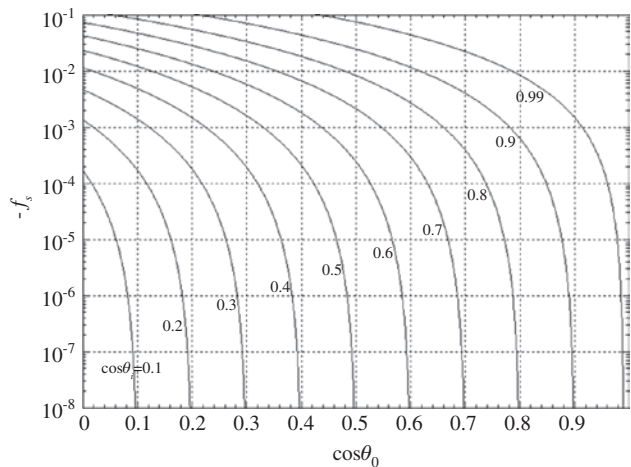


Figure 11: Shape factor (dimensionless volumetric flow rate), f_s vs. $\cos\theta_o$ and parameterized with $\cos\theta_i$ [Eq. (71)].

For this same die, the cylindrical approximations [Eqs. (73) and (74)] give:

$$f_c^i \approx -0.0253 \quad (114)$$

$$f_c^o \approx -0.0168 \quad (115)$$

and the Liang approximation [Eq. (6)] gives:

$$f_L \approx -0.187 \quad (116)$$

Combining Eq. (71) with $\Delta \mathcal{P} \equiv \Delta p r_i / (\mu V_{\max})$ and $\mathcal{Q} \equiv Q / (V_{\max} r_i^2)$ from Table 3 and rearranging gives the pressure drop:

$$-\Delta p = \frac{-Q\mu(1-\kappa^3)}{3\pi r_i^3 f_s} = \frac{-\rho Q\mu(1-(r_i/r_o)^3)}{3\pi r_i^3 f_s} \quad (117)$$

Inserting the given die geometry, physical properties and Eq. (113) into Eq. (117):

$$\begin{aligned} -\Delta p &= \frac{-(-0.0100 \text{ kg/s})1.10 \times 10^7 \text{ Pa}\cdot\text{s}(1-(0.0500/0.130)^3)}{3\pi(900 \text{ kg/m}^3)(0.0500 \text{ m})^3(-0.00257)} \\ &= -3.81 \times 10^7 \text{ Pa} \end{aligned} \quad (118)$$

which the engineer must use to get the required throughput.

(ii) Using Eqs. (106), (90) and $P \equiv 2\lambda\Delta p/\mu$, $\mathcal{R} \equiv r - r_i/r_o - r_i$ and $\xi \equiv \theta - \theta_i/\theta_o - \theta_i$ from Table 3, she gets the expression for the temperature rise in the converging die:

$$T - T_0 = \left[\frac{2\Delta p \kappa^3}{\rho \tilde{C}_p (1-\kappa^3)} \right] \left[1 - \frac{r_o^3}{r^3} \right] A \quad (119)$$

and since the temperature peaks at r_i :

$$T_{\max} - T_0 = \frac{-2A\Delta p}{\rho \tilde{C}_p} \quad (120)$$

Inserting the physical properties, A and Eq. (118) into Eq. (120), she gets:

$$T_{\max} - T_0 = \frac{-2(-0.0941)3.81 \times 10^7 \text{ Pa}}{(900 \text{ kg/m}^3)1.60 \times 10^3 \text{ J/kg}\cdot\text{C}} = 4.98^\circ\text{C} \quad (121)$$

which she can then add to the temperature rise for the die land, to see if her polymer extrudate will exceed its degradation point.

At the end, she verifies the two flow conditions: $Re \ll 1$ and $Pé \ll 1$. Using Eqs. (130):

$$Re \equiv \frac{\rho V_{\max} r_i}{\mu} \quad (122)$$

where V_{\max} is calculated using Eq. (42):

$$V_{\max} = |v_r(r_i, \theta_{\min, v_r})| = \left| \frac{\Delta p A r_i}{2\mu(1-(r_i/r_o)^3)} \right| \quad (123)$$

$$\begin{aligned} V_{\max} &= |v_r(0.0500 \text{ m}, 20.2^\circ)| \\ &= \left| \frac{3.81 \times 10^7 \text{ Pa}(-0.0941)0.0500 \text{ m}}{2(1.10 \times 10^7 \text{ Pa}\cdot\text{s})(1-(0.0500/0.130)^3)} \right| \\ &= 0.0086 \text{ m/s} \end{aligned} \quad (124)$$

She gets, after inserting Eq. (124) and the physical properties into Eq. (122):

$$Re = \frac{(900 \text{ kg/m}^3)0.0086 \text{ m/s}(0.0500 \text{ m})}{1.10 \times 10^7 \text{ Pa}\cdot\text{s}} = 3.52 \times 10^{-8} \quad (125)$$

which is $\ll 1$.

She then uses Eq. (92) and Table 2 to get:

$$Pé = \frac{k\mu(r_o - r_i)}{(\rho \tilde{C}_p)^2 r_o^3 (T_{\max} - T_0)} \quad (126)$$

Inserting Eq. (121) and the physical properties into Eq. (126) gives:

$$\begin{aligned} Pé &= \frac{(0.1 \text{ W/m})1.10 \times 10^7 \text{ Pa}\cdot\text{s}(0.130 \text{ m} - 0.0500 \text{ m})}{(900 \text{ kg/m}^3)^2(1.60 \times 10^3 \text{ J/kg}\cdot\text{C})^2(0.130 \text{ m})^3 4.98^\circ\text{C}} \\ &= 3.88 \times 10^{-6} \end{aligned} \quad (127)$$

which is also $\ll 1$.

This specific worked example happens to be the one we chose to illustrate in Figure 1.

6 Conclusion

This paper attacks the problem relevant to the connection between a plastics extruder and a pipe extrusion die: the pressure-driven flows, converging or diverging, through the annulus between coapical coaxial cones. Using the transport phenomena approach we arrive at (1) an exact solution for the velocity profile [Eq. (67)] which we integrate to get (2) the throughput per unit pressure drop [Eq. (75)] and (3) the temperature rise [Eqs. (106) and (107)]. We care about this rise because it often governs maximum throughput, since pipe makers must keep the melt from degrading. Equation (75) and Eqs. (106) and (107) are the two main results of this work, which we cast in dimensionless terms (see Table 3) and which we illustrate in Figures 8, 9 and 11.

Our first main result, the exact solution for the throughput [Eq. (75)] is subject to the dimensionless constraints on the geometry, $A \ll 1$, on the flow field, $Re \ll 1$

(see Appendix 7.1), that is that fluid inertia be negligible. We find that these constraints normally apply to plastic pipe extrusion. Our second main result, the exact solution for the temperature rise [Eqs. (106) and (107)], is subject to the dimensionless constraints, $A \ll 1$, and on the flow field, $Pé \ll 1$, that is, that latitudinal conduction is negligible relative to radial convection. We find this exact solution for the temperature rise to be consistent with isothermal, inner and outer die walls, and we thus calculate the corresponding heat flux requirements for cooling [Eqs. (109)–(112)]. To teach practitioners how to use our main results, we crafted Figure 11 and our two-part worked example (see Section 5).

We are unaware of any temperature rise measurements on flow through conical annuli, with which Eqs. (106) and (107) might be compared. Whereas we do find flow rate measurements reported for non-Newtonian fluids pumped through converging dies [6], we find none for Newtonian fluids, with which Eq. (75) might be compared. Moreover, the non-Newtonian flow rate measurements that we do find [6] are for only a slight convergent conical die ($\theta_o \approx 12^\circ$, $\theta_i = 10^\circ$ and $\kappa \approx \frac{1}{2}$).

In this paper, we have focused on the extrusion of pipe, or tubing, or catheters. We close by noting that our work will be at least as useful to those designing diverging dies for blow molding [21–24].

Acknowledgments: A. Jeffrey Giacomini is indebted to the Faculty of Applied Science and Engineering of Queen's University at Kingston, for its support through a Research Initiation Grant. This research was undertaken, in part, thanks to support from the Canada Research Chairs program of the Government of Canada for the Natural Sciences and Engineering Research Council of Canada Tier 1 Canada Research Chair in Rheology. Georges R. Younes acknowledges Mrs. Nadia Moufarrej of the Faculty of Engineering and Architecture of the American University of Beirut for her invaluable support.

7 Appendices

7.1 Reynolds number

In this paper, to obtain our main results [Eq. (75)], we neglected fluid inertia. In this appendix, we closely examine this assumption by defining the Reynolds number for the pressure-driven flows, converging or diverging, through the annulus between coapical coaxial

cones. Retaining the inertial terms in Eq. (18) and still neglecting gravity, and since $p(r)$, gives:

$$\frac{\rho C}{\mu r} = \frac{r^4}{2C\mu} \frac{dp}{dr} \cdot \frac{1}{2C\sin\theta} \frac{d}{d\theta} \left(\frac{dC}{d\theta} \sin\theta \right) \quad (128)$$

which, using Table 3, can be rewritten as:

$$\text{Re} \kappa \mathcal{C} \Delta \mathcal{P} = \frac{r^4 [R(1-\kappa) + \kappa]}{2C\mu} \frac{dp}{dr} \cdot \left(\frac{R(1-\kappa) + \kappa}{2C\sin\theta} \right) \frac{d}{d\theta} \left(\frac{dC}{d\theta} \sin\theta \right) \quad (129)$$

in which we have uncovered the Reynolds number for pressure-driven flows through the annulus between coapical coaxial cones:

$$\text{Re} \equiv \frac{\rho V_{\max} r_i}{\mu} \quad (130)$$

Since for most polymeric liquids the viscosity μ is large, $\text{Re} \ll 1$.

7.2 Latitudinal symmetry of \mathcal{C}

Using Table 3 to adimensionalize Eq. (49) and rearranging we get:

$$\frac{\partial \mathcal{P}}{\partial \xi} = \frac{2\kappa^3}{[\mathcal{R}(1-\kappa) + \kappa]^3} \frac{d\mathcal{C}}{d\xi} \quad (131)$$

Since $\mathcal{P}(\mathcal{R})$:

$$0 = \frac{1}{[\mathcal{R}(1-\kappa) + \kappa]^3} \frac{d\mathcal{C}}{d\xi} \quad (132)$$

and thus:

$$\frac{d\mathcal{C}}{d\xi} = 0 = \frac{d\mathcal{C}}{d\theta} \quad (133)$$

since \mathcal{C} is proportional to \mathcal{C} and since ξ is just normalized θ .

References

- [1] Bird RB, Stewart WE, Lightfoot EN. *Transport Phenomena*. 1st ed., Wiley: New York, 1960.
- [2] Bird RB, Stewart WE, Lightfoot EN. *Transport Phenomena*, 2nd ed., John Wiley & Sons: New York, 2002.
- [3] Parnaby J, Worth RA. *Proc. Inst. Mech. Eng.* 1974, 188, 357–364. Erratum: In Eq. (4), η_o should be $\eta_o/\dot{\gamma}_o$.
- [4] Dijkstra JF, Savenije EPW. *Rheol. Acta* 1985, 24, 105–118.
- [5] Kollitawong C, Giacomini AJ. *Polym.-Plast. Technol. Eng.* 2001, 40, 363–384.

- [6] Liang JZ. *Polym. Test.* 2003, 22, 497–501. Erratum: In Table 1, the unit for K should be $(Pa\ s^n)$ instead of $(Pa\ s)$. Addendum: In Eq. (11) in [16] and Eq. (6) in this paper, $\theta [=]$ rad.
- [7] Kolitawong C, Kananai N, Giacomini AJ, Nontakaew U. *J. Non-Newtonian Fluid Mech.* 2011, 166, 133–144.
- [8] Githuku DN, Giacomini AJ. *J. Eng. Mater. Technol.* 1992, 114, 81–83.
- [9] Githuku DN, Giacomini AJ. *J. Eng. Mater. Technol.* 1993, 115, 433–439.
- [10] Githuku DN, Giacomini AJ. *Int. Polym. Process.* 1992, 7, 140–143.
- [11] Githuku DN, Giacomini AJ. In *Proceedings, First International Conference on Transport Phenomena in Processing, Pacific Institute for Thermal Engineering, Honolulu, HI (March 22-26, 1992)*, Guceri SI, Ed., Technomic Publishers Inc.: Lancaster, PA, 1992, pp 997–1012.
- [12] Githuku DN, Giacomini AJ. *Proceedings, Polymer Processing Society, Seventh Annual Meeting*, Hamilton, Canada, April 21–24, 1991, p 260.
- [13] Giacomini AJ, Doshi SR. In *SPE Tech. Paper, XXXIV, Society of Plastics Engineers, Proc. 46th Annual Tech. Conf. & Exhib.*, Atlanta, GA, 1988, pp 38–40.
- [14] Kolitawong C, Giacomini AJ, Nontakaew U. *Polym. Eng. Sci.* 2013, 53, 2205–2218.
- [15] Pittman JFT, Whitham GP, Beech S, Gwynn D. *Int. Polym. Process.* 1994, 9, 130–140.
- [16] Pittman JFT, Farah IA. *Plast. Rubber Compos. Process. Appl.* 1996, 25, 305–312.
- [17] Pittman JFT, Whitham GP, Farah IA. *Polym. Eng. Sci.* 1995, 35, 921–928.
- [18] Pittman JFT, Farah IA. Computer Simulation of the Cooling Process in Plastic Pipe Manufacture, Including Sag, Thermal Stress and Morphology, *Proc. Plastic Pipes IX (Inst. Materials) Edinburgh* 1995, 364–371.
- [19] Saengow C, Giacomini AJ, Kolitawong C. *J. Non-Newtonian Fluid Mech.* 2015, 223, 176–199.
- [20] Middleman S. *Fundamentals of Polymer Processing*. McGraw-Hill: New York, 1977, pp 120–121. Addendum: In Problem 5-37, $Y = y_0/y_1 = y_0/(y_0 + L)$, $\kappa = r_i/r_o = \tan \alpha / \tan \beta$ and $R_0 = y_0 \tan \beta$.
- [21] Stanfill KO. Measurement of Nonlinear Viscoelastic Shear Properties of High Density Polyethylene Programmed Parison Blow Molding Resins Using a Unique Mode Switch Test, Master's Thesis, Texas A&M University, Mechanical Engineering Dept., College Station, TX (March, 1992).
- [22] Giacomini AJ, Jeyaseelan RS, Stanfill KO. *Polym. Eng. Sci.* 1994, 34, 888–893.
- [23] Garcia-Rejon A, Dealy JM. *Polym. Eng. Sci.* 1982, 22, 158–165.
- [24] Luo XL, Mitsoulis E. *J. Rheol.* 1989, 33, 1307–1327.